International Journal of Automotive Technology, Vol. 8, No. 2, pp. 165–177 (2007)

1229-9138/2007/033-05

DETAILED EXAMINATION OF INVERSE-ANALYSIS PARAMETERS FOR PARTICLE TRAPPING IN SINGLE CHANNEL DIESEL PARTICULATE FILTER

S.-C. JUNG[1], J.-S. PARK[1] and W.-S. YOON[2]*

[1]The Graduate School, Department of Mechanical Engineering, Yonsei University, Seoul 120-749, Korea
[2]Department of Mechanical Engineering, Yonsei University, Seoul 120-749, Korea

(Received 4 April 2006; Revised 28 February 2007)

ABSTRACT–Predictions of diesel particulate filtration are typically made by modeling of a particle collection, and providing particle trapping levels in terms of a pressure drop. In the present study, a series of single channel diesel particulate filter (DPF) experiments are conducted, the pressure traces are inversely analyzed and essential filtration parameters are deducted for model closure. A DPF filtration model is formulated with a non-linear description of soot cake regression. Dependence of soot cake porosity, packing density, permeability, and soot density in filter walls on convective-diffusive particle transportation is examined. Sensitivity analysis was conducted on model parameters, relevant to the mode of transition. Soot cake porosity and soot packing density show low degrees of dispersion with respect to the Peclet number and have asymptotes at 0.97 and 70 kg/m^3, respectively, at high Peclet number. Soot density in the filter wall, which is inversely proportional to filter wall Peclet number, controls the filtration mode transition but exerts no influence on termination pressure drop. The percolation constant greatly alters the extent of pressure drop, but is insensitive to volumetric flow rate or temperature of exhaust gas at fixed operation mode.

KEY WORDS : Diesel Particulate Filters (DPF), Soot loading, Pressure drop, Filtration

1. INTRODUCTION

Presently, particle trapping by DPF is accepted as a general practice to cope with diesel particulate matter (PM) emission. Similar to typical particle filtration methods, particulate matters piled inside DPF gradually hinder fluent gas streaming and cause significant augmentation of back pressures or even clog the gas exhaust through the tail pipe; therefore, as a simple remedy against this innate defect, the DPF is cleaned regularly before it exceeds the permitted limit for PM collection (or removal). Thermal or catalytic regeneration is a practical cure. In regards to signaling, the termination of trapping and the switch-on to regeneration, collection levels inside the DPF must be evaluated. Direct measument of instant PM mass is desirable. However, gauging the instant PM mass in on-board DPF is frequently avoided because of its heavier cost for precision measurement. In measuring the instant PM mass with economy, pressures of exhaust flows entering and exiting DPF are recorded to find the pressure difference which shows an approximate linear dependence to instant PM mass and provides the moment of transit to regeneration. Mode transition is conducted on the basis of data for pressure drops, and thus a principal aim of DPF modeling shifts to correct prediction of evolving exit pressures. Since net effect of phenomena is measured only by pressure, and the physics of participating processes involves orderly disparate length scales, modeling comprising such diversity is inappropriate and the complexities must be alleviated. Even a lab-scale experiment can hardly resolve the complexities inherent in the coupling mechanism since the controlling phenomena are numerous and of almost equal importance in their individual physics. Studies have focused on correctly describing essential physics associated with PM collection, sorting principal routes reaching pressure drop, and enveloping for on-board use.

Modeling of DPF performance was pioneered by Bissett (1984). In this simple model, formulation of essential participants in filtration such as flow field, soot cake piling on the filter wall, and even thermal regeneration were introduced. Among studies inheriting the general structure of Bisset's model, Konstandopoulos and Johnson's (1989) work placed emphasis on comprehensive descriptions of filtration characteristics and pressure drop, thus making substantial progress for practical use in the industry.

*Corresponding author. e-mail: wsyoon@yonsei.ac.kr

Opris and Johnson (1998a, 1998b) attempted a two-dimensional computational model treating the filtration after due consideration of channel flows and soot regeneration. They resolved the filtration phenomena by breaking down the particle trapping by the collector into Brownian diffusion, inertial impaction, and direct interception, and proposed an effective porosity concept. Konstandopoulos *et al.* (2001, 2002) extended their model by adding inertial contributions to the pressure drop, and also made an effort to reveal microstructure effects of the soot cake and correlate the cake porosity to the particle Peclet number. Huynh *et al.* (2003) proposed a rather rigorous filtration model which includes the variation of filtration velocity along a longitudinal direction in a DPF channel. Also proposed was a regeneration model for catalyzed wall-flow DPF. Kladopoulou *et al.* (2003) proposed a lumped parameter model with validation comparing typical filtration parameters such as pressure drop, mass of collected particulate matter, and temperature for regeneration.

One generally seeks to establish a robust and accurate DPF model when predicting DPF filtration. Here, the performance parameters such as pressure drop and rate of soot mass collection/removal is of primary interest. However, formulation in terms of parametric expression such as soot cake permeability, soot cake density, soot density in the filter wall, and the percolation constant, commonly induces a closure problem due to the lack of theoretical routes linking microscopic filtration physics to the system factors. In order to close the model formulation, precise numerical figures must be provided, and an inverse-analysis of filtration measurements is considered to be the solution at hand. In the present study, a series of single channel DPF experiments are conducted, the pressure traces are inversely analyzed and the essential filtration parameters are deducted. A DPF filtration model is freshly formulated with non-linear description of soot cake regression. We examine dependence of essential filtration parameters controlling the PM trapping (soot cake porosity, packing density, permeability, and soot density in filter wall) on a convective-diffusive particle transportation mechanism is examined. Parametric sensitivity analysis of model parameters essential to filtration mode transition is also was performed.

2. PRESSURE DROP MODEL

The advancement in the study of DPF filtration modeling is largely attributed to Konstandopoulos and Johnson (1989; Konstandopoulos *et al.*, 2000) and their colleagues. Variability of the phenomena associated with PM collection was treated in a rigorous and comprehensive fashion, and the prediction was validated with data from precision measurements in fairly good agreement over a variety of test conditions. Their method may be credited to setting industrial standards for DPF filtration, and thus essentials of the present study repeat the general frame of their model; the pressure drop through soot cake and filter wall is formulated by Darcy's law and the collection of particulate matter by packed beds is modeled by a unit collector filtration theory. The pressure drops through the filter wall and soot cake are written in view of Darcy's law and simply superimposed into the net equation:

$$\Delta p=\frac{\mu}{k_{wall}}u_{wall}w+\frac{\mu}{k_{soot}}\int_0^{w_s}u_{soot}(x)dx \tag{1}$$

where, Δp, k_{wall}, k_{soot}, u_{wall}, u_{soot}, w, w_s, and μ are pressure drop, filter wall permeability, soot cake permeability, filter wall filtration velocity, soot cake filtration velocity, filter wall thickness, soot cake thickness, and viscosity of exhaust gas, respectively. In Equation (1), inlet/outlet channel friction loss, contraction/expansion inertial loss, Forchheimer effects reflecting the pressure loss due to high filtration velocity and compressibility at large pressure drop are not considered since their effects are frequently minimal. Since the Reynolds number of particle laden gas flows inside the filter is very low, that is, highly dissipative, the pressure gradient across the filter wall is very steep due to significant hydraulic loss, and its extent depends on the situation of PM deposition defined by local filter wall permeability with altered wall porosity.

$$\Delta p=\mu u_{wall}dw\sum_i\frac{1}{k_{wall,i}}+\frac{\mu}{k_{soot}}\int_0^{w_s}u_{soot}(x)dx \tag{2}$$

where dw is the thickness of a slab when the filter wall is assumed to be divided equally into n slabs, and thus $k_{wall,i}$ is the permeability of the ith slab (Konstandopoulos *et al.*, 2000; Kladopoulou *et al.*, 2003). If the change of soot cake width is negligible and the flows are uniform inside, permeability and density of the soot cake can be combined into their product, a single parameter of hydrodynamic resistance factor ($k_{soot}\rho_{soot,c}$) (Konstandopoulos *et al.*, 2005).

$$\Delta p=\mu u_{wall}dw\sum_i\frac{1}{k_{wall,i}}+\frac{\mu u_{soot}}{k_{soot}\rho_{soot,c}}\frac{m_c}{A_{filt}} \tag{3}$$

Here, m_c is the mass of soot cake, $\rho_{soot,c}$ is the density of soot cake, respectively. A_{filt} is filtration area of the soot cake given by

$$A_{filt}\approx 4\alpha L \tag{4}$$

Where α and L are cell width and length of the filter, respectively. Assuming the filtration velocities through soot cake and filter wall are approximately equal ($u_w\approx u_{wall}\approx u_{soot}$),

$$\Delta p=\mu u_w dw\sum_i\frac{1}{k_{wall,i}}+\frac{\mu u_w}{k_{soot}\rho_{soot,c}}\frac{m_c}{A_{filt}} \tag{5}$$

3. SINGLE CHANNEL DPF EXPERIMENTS

Owing to its own geometric situation tailored for easy packing and higher filtration efficiency, the DPF of cylindrical configuration is not excluded from steep temperature gradients along longitudinal and lateral directions, resulting in intensive conductive thermal diffusion and significant unevenness of local temperatures. This provides a primary cause for the use of heat-resistant base materials for the DPF structures. In addition, a less uniform map of volumetric flow rate distributions on the cross sectional area of channels yields uneven soot particle depositions. Spatial dependence on filtration characteristics is evident thus, treatment of this geometry on multidisciplinary situations can hardly be concluded in one frame for a solution. And thus, isolating spatial parameters for less uncertainties and raising reliability of experimental data, the use of a single filtration element (one channel of DPF) is advisable and certainly provides a starting point. For a coherent account, one channel of commercialized DPF (Corning EX-80 DPF) was wire-cut and asperities were removed by precision grinding. Figure 1 illustrates general profiles of the exhaust gas flows

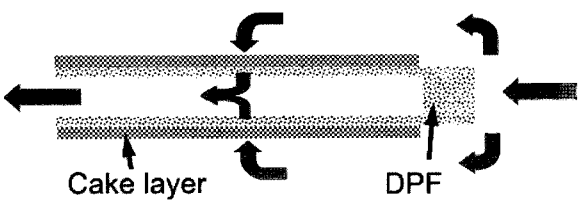

Figure 1. Profile of running diesel exhaust flows and PM trapping through SC-PDF.

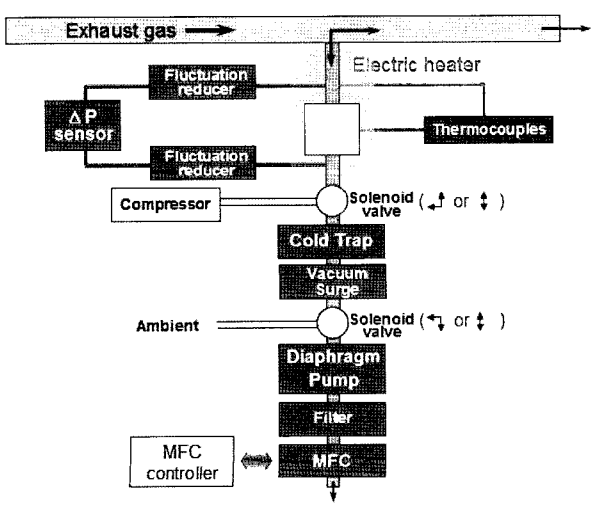

Figure 2. Schematic of DPF test by partial flow system equipped with MFC for regulating bifurcated exhaust gas flow rate and electric heater for temperature control.

Table 1. Operation modes of single channel DPF tests.

	sLPM	T [°C]	u_w [m/s]	$\dot{m}_{soot}$ [kg/s]	MW [kg/kmol]
IDI engine, 1250 rpm, 80% load					
Mode 1	1.08	260	0.046	0.3833×10^{-9}	29
Mode 2	1.61	260	0.069	0.5833×10^{-9}	
Mode 3	2.15	260	0.092	0.7667×10^{-9}	
Mode 4	4.30	260	0.184	1.5333×10^{-9}	
CRDI engine, 1500 rpm, 28% load					
Mode 5	1.08	260	0.046		32
Mode 6	1.08	300	0.049	0.3333×10^{-9}	
Mode 7	1.08	340	0.052		
Mode 8	1.61	260	0.068		
Mode 9	1.61	300	0.073	0.5×10^{-9}	
Mode 10	1.61	340	0.078		
Mode 11	2.15	260	0.091		
Mode 12	2.15	300	0.098	0.9833×10^{-9}	
Mode 13	2.15	340	0.104		
CRDI engine, 1500 rpm, 42% load					
Mode 14	1.09	260	0.046		32
Mode 15	1.09	300	0.050	0.3×10^{-9}	
Mode 16	1.09	340	0.053		
Mode 17	2.17	260	0.092		
Mode 18	2.17	300	0.099	0.6×10^{-9}	
Mode 19	2.17	340	0.105		

through a fabricated single channel and Table 3 provides a summary of material properties and geometry of the specimen.

A naturally aspirated Indirect Injection (IDI) engine with a displacement volume of 2957cc and a turbocharged CRDI (common rail direct injection) engine with a displacement volume of 1991cc supply the PM contaminated emission. PM loading tests are conducted for three different engine operating conditions (80% load at 1250 rpm, 28% load at 1500 rpm, and 42% load at 1500 rpm, respectively). Exhaust gas is bifurcated through a secondary pipe and diverted into SC-DPF units (Figure 2). Volumetric flow rates of exhaust gas are regulated by mass flow controller (MFC) and electric heater functions to sustain the filter temperature in a targeted size range. With this partial flow system, in which three major flow parameters associated with pressure loss, PM concentration, exhaust volumetric flow rate (in terms of standard condition, sLPM), and temperature are controlled separately, nineteen modes of loading operation are examined. Modes of single channel DPF tests are summarized in Table 1 in which T, u_w, $\dot{m}_{soot}$ and MW are exhaust

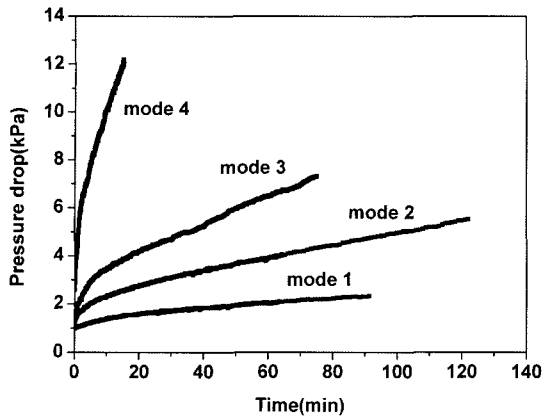

Figure 3. Evolutions of SC-DPF pressure drop due to different engine operation modes. (Mode 1 through 4: IDI engine at 1250 rpm-80% load).

temperature, filtration velocity, mass flow rate of soot particles, and molar mass of exhaust gas, respectively. Because soluble organic fractions (SOFs) exist in a gaseous state at high temperature above 190°C, the SOF is removed from the sampled exhaust gas by Soxhlet extraction. Filtration velocity is obtained simply by dividing exhaust volumetric flow rate by filtration area (A_{filt}). Here, the volumetric flow rate at standard state (20°C, 1 atm) should be properly corrected to include volumetric expansion due to temperature rise in SC-DPF. Prior to PM loading tests with exhaust gas, uncontaminated air tests in order to estimate pure filter permeability and contraction/expansion inertial loss coefficient were conducted and result in the reference values of 8.3×10^{-13} and 1.55, respectively.

Figures 3 through 5 portray evolving DPF pressure drops in terms of engine operation modes. A straight-line segment on the Δp–t plots implies that the functional relationship between the variables is linear, but with deviation during the initial period of evolution, that is, a deep bed mode. Importantly, these traces are the plots of pressure drops by filter wall and soot cake only, obtained by subtracting pressure losses due to inlet/outlet channel friction and contraction/expansion inertial flows from the raw data. The mathematical descriptor of pressure drop, which includes all terms participating in the pressure loss and the data processing methods of the previous study (Konstandopoulos, 2003) was adopted to seek pressure drop curves for filter wall and soot cake. Detailed accounts on the present experimental strategy is found in references (Park, 2005; Park *et al.*, 2005).

4. INVERSE-ANALYSIS FOR MODEL PARAMETERS

Formulation for DPF filtration modeling can only be closed by providing aforementioned filtration parameters which link essential microscopic phenomena to the pressure drop with precise numerical figures. However, exact or approximate formulae describing this critical relation is neither currently present nor expected to be provided in near future. An inverse-analysis of measured pressure data is further feasible to evaluate the solution at hand, in order to circumbent this dilemma. Resultant numeric data are much easier to deal with in subsequent use and even give the first glimpse of the degree of difficulties on filtration. Parameters to be determined include permeability of soot cake (k_{soot}), density of soot cake ($\rho_{soot,c}$), soot density in the filter wall ($\rho_{soot,w}$), and the percolation constant (ψ). Permeability and density of soot cake define the cavity density of the soot cake layer over the channel wall surface (Figure 1) and their product is equivalent to the hydraulic resistance due to particles piled on the surface of the channel. A previous study has shown that these two parameters are strongly correlated by soot cake Peclet number, a dimensionless number which is the ratio of convective to diffusive transport of the particle, which can be empirically evaluated with the assistance of discrete particle simulation (Konstandopoulos *et al.*, 2002). Soot density in the filter wall governs the growth rate of the collector size, thus controling the wall porosity, pressure-drop evolution, and determines the extent of PM collection efficiency in the deep-bed filtration regime. During the period of deep-bed filtration, bulky PM trapping is made by the collecting entities in the filter wall. As the process evolves, however, a gradually thickened PM layer due to lasting PM deposit on the collector surface causes a reduction of the cavity volume, hinders the fluent flows by clogging narrow flow passage, and readily increases the pressure drop. Once the collectors in the vicinity of upper surface of the porous filter wall are completely loaded, filtration mode transits into the particle piling (soot cake) mode. This situation may simply be mimicked by saturation of the particle loading in the filter wall, represented by the percolation constant which defines the size of a completely loaded collector. A thorough review of the pressure drop model on the ground of definitions of the soot density in the filter wall and the percolation constant is found in the references (Konstandopoulos *et al.*, 2000; Kladopoulou *et al.*, 2003). These essential parameters can only be evaluated by experiments, and thus the soot density in the filter wall and percolation constant are considered to be true model parameters on which no physical interpretation is drawn; empirical tuning is imposed to mimick the unit collector filtration theory. The permeability factor appears in Equation (5) only in the form of a product of $\rho_{soot,c}k_{soot}$, and the hydrodynamic resistance factor ($k_{soot}\rho_{soot,c}$) replaces this product for simplicity.

In the present study, a non-linear regression scheme

Table 2. Filtration parameters determined by non-linear regression calculation.

	T [°C]	u_w [m/s]	$\rho_{soot,w}$ [kg/m^3]	ψ	$k_{soot}\rho_{soot,c}$ [kg/m]
IDI engine, 1250 rpm, 80% load					
Mode 1	260	0.046	2.87612	0.88938	3.5953×10^{-12}
Mode 2	260	0.069	4.39683	0.89454	3.3994×10^{-12}
Mode 3	260	0.092	3.38055	0.89091	2.711×10^{-12}
Mode 4	260	0.184	1.90555	0.88143	1.4373×10^{-12}
CRDI engine, 1500 rpm, 28% load					
Mode 5	260	0.046	13.77103	0.93262	5.2889×10^{-12}
Mode 6	300	0.049	12.76058	0.93129	5.4386×10^{-12}
Mode 7	340	0.052	9.35385	0.9273	4.3866×10^{-12}
Mode 8	260	0.068	8.85398	0.93347	3.7575×10^{-12}
Mode 9	300	0.073	6.21707	0.92886	2.8142×10^{-12}
Mode 10	340	0.078	3.05377	0.925	2.6782×10^{-12}
Mode 11	260	0.091	4.66157	0.93431	3.8592×10^{-12}
Mode 12	300	0.098	3.0481	0.9298	2.9671×10^{-12}
Mode 13	340	0.104	3.36377	0.93048	4.0043×10^{-12}
CRDI engine, 1500 rpm, 42% load					
Mode 14	260	0.046	18.82842	0.9425	6.1628×10^{-12}
Mode 15	300	0.050	18.71637	0.94	6.4751×10^{-12}
Mode 16	340	0.053	17.44042	0.93726	5.8557×10^{-12}
Mode 17	260	0.092	8.53134	0.93848	3.2345×10^{-12}
Mode 18	300	0.099	8.057	0.9357	3.5563×10^{-12}
Mode 19	340	0.105	7.03917	0.93271	3.5823×10^{-12}

which utilizes the Levenberg-Marquardt method (Press *et al.*, 1992), a higher-order numerical technique to determine unknowns which minimize the values of non-linear function, is freshly introduced for inversely analyzing the experimental data. Solution convergence was apparent and results are shown in Table 2. In the present inverse-analysis, it is crucial whether the extracted inverse-analysis parameters due to iterative numerical calculations comprising linear and non-linear parts of the pressure curve come within physical proper range with uniqueness. Comparison with numerical solutions by other calculation strategies for the same filtration procedures properly validate the present non-linear regression scheme of physical correctness and uniqueness of the solutions. A set of experimentally determined filtration parameters in Table 2 is repeatedly applied to a series of computations, aiming at investigating DPF hydraulics (pressure drops) due to different operation modes. Figures 6 through 8 compare the predicted data with measured pressure transients and agreements are remarkable. The model fits quite well for the practice demonstrating validity. However, this outstanding performance is heavily indebted to

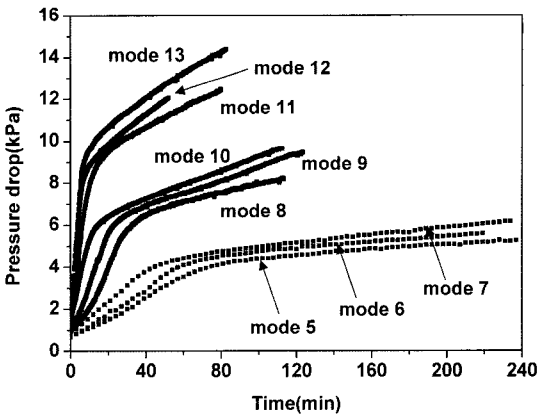

Figure 4. Evolutions of SC-DPF pressure drop due to different engine operation modes. (Mode 5 through 13: CRDI engine at 1500 rpm-28% load).

deductions from a set of experimental data by inverse-analysis, and naturally such a lack of distinct physics causes inconsistency in variance due to different modes. Table 3 gives input parameters for the SC-DPF pressure drop model. In view of its own definition, hydrodynamic resistance factor can be evaluated directly from pressure-drop curves. During a period of cake filtration mode, entire PM entering the DPF is piled on preceding colleagues, while no further collecting nor alteration of hydraulic characteristics is made in the filter wall. Hence, an overall pressure drop increases linearly in proportion to the increase in the thickness of the soot cake layer. This general tendency is repeated in the present single channel DPF experiments (Figure 3, 4 and 5), and thus a temporal gradient of the pressure drop in the cake filtration regime may conveniently be expressed in terms of the hydrodynamic resistance factor. Differentiating Equation (5) by time,

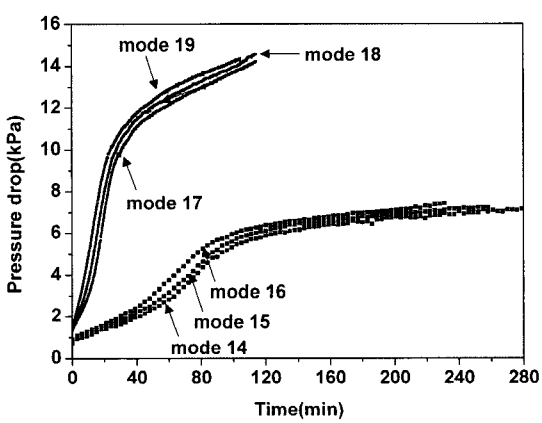

Figure 5. Evolutions of SC-DPF pressure drop due to different engine operation modes. (Mode 14 thorough 19: CRDI engine at 1500 rpm, 42% load.

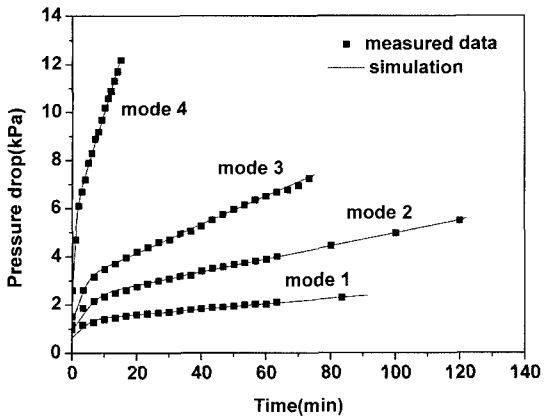

Figure 6. Experimental filter pressure drops compared with the prediction of calibrated model (solid line) for engine operation modes 1 through 4.

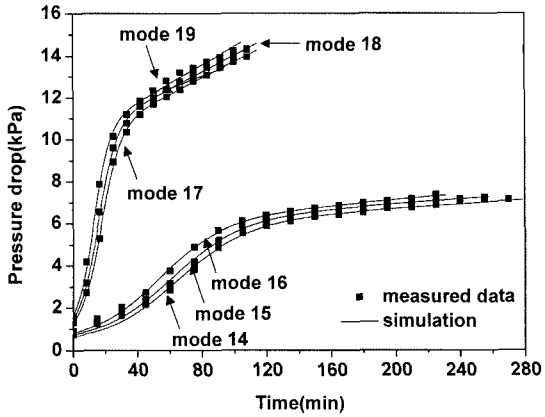

Figure 8. Experimental filter pressure drops compared with the prediction of calibrated model (solid line) for engine operation modes 14 through 19.

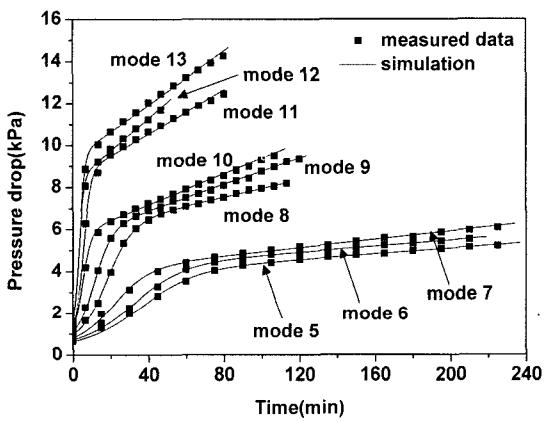

Figure 7. Experimental filter pressure drops compared with the prediction of calibrated model (solid line) for engine operation modes 5 through 13.

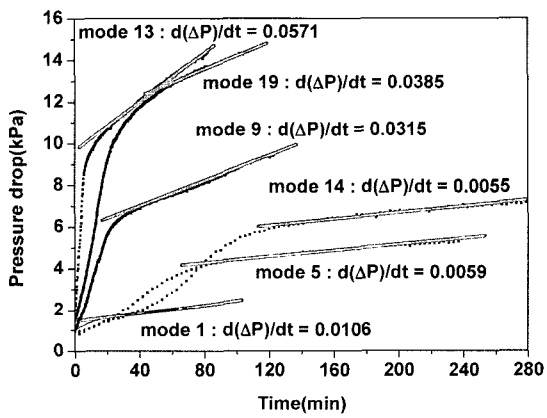

Figure 9. Slopes of increasing pressure drops at soot cake filtration regime in terms of engine operation modes of 1, 5, 9, 13, 14, and 19 (the slope is for the linear portion of soot cake filtration regime).

$$\frac{d\Delta p}{dt}=\frac{\mu u_w}{k_{soot}\rho_{soot,c}}\frac{1}{A_{filt}}\frac{dm_c}{dt} \tag{6}$$

$$\frac{dm_c}{dt}=\dot{m}_{soot} \tag{7}$$

dm_c/dt in Equation (6) (or $\dot{m}_{soot}$ in Equation (7)) is linearly related to hydraulic resistance ($k_{soot}\rho_{soot,c}$) when μ, u_w, and A_{filt} are constant, and thus the changes in the pressure drop is instantly determined by linearly fitting the measured data, by simply finding a slope of a straight portion of curves (Figure 9). In Table 4, hydrodynamic resistance factors determined by inverse-analysis of experiments and linear curve-fitting are shown for 6 operation modes. Taking vastly different exhaust situations into account, disagreement is only marginal so that the present prediction method employing a non-linear regression scheme can be asserted as valid in practice.

5. PM LOADING CHARACTERISTICS

As noted previously, the pressure drop due to hydraulic resistance of soot cake is exploited as an important and convenient indicator, probing instant degree of mass loading. However, in order for modeling microscopic phenomena in terms of this pressure drop only, the model parameters should properly reflect the variability of the routes essential to particle trapping. Porosity of the soot cake, a measure of relative ease of flow permeability and a macroscopic geometrical property describing soot layer packing structure as well, is heavily dependent on the extent of convective-diffusive transportation of the soot aggregates and the size of primary soot particles. Brownian random motions of particles contribute to augmenting pore cavities, whereas convective transports along the

Table 3. Geometry of states in SC-DPF to be examined.

Parameter	Description
Exhaust condition	
Exhaust temperature	260°C, 300°C, 340°C
Filtration velocity	0.046 m/s~0.184 m/s
Particulate mass flow rate	0.3×10^{-9} kg/s~ 1.5333×10^{-9} kg/s
Molar mass of exhaust	29 kg/kmol, 32 kg/kmol
Exhaust density	Assumed to be air density
Exhaust viscosity	(Konstandopoulos, 2003)
Aggregate particle size	Assumed to be 0.1 μm
Filter geometry & Property	
Channel length	95 mm
Channel width	2.1 mm
Wall thickness	0.4318 mm
Wall porosity	48%
Mean pore size	12.5 μm
Clean filter wall permeability	8.3×10^{-13} m^2
Parameters to close pressure drop model	
Hydrodynamic resistance factor	*
Soot density in the filter wall	*
Percolation constant	*
Numerical code control parameter	
Time step	5 sec
Number of discretized slab (filter wall)	5

*is to be filled with the data by inverse-analysis of the measurements (Table 2)

Table 4. Error estimation of predicted to measured hydrodynamic resistance factors.

	$k_{soot}\rho_{soot,c}$ non-linear regression	$k_{soot}\rho_{soot,c}$ linear fitting	diff (%)
Mode 1	3.5953×10^{-12}	3.7740×10^{-12}	4.7
Mode 5	5.2889×10^{-12}	5.8960×10^{-12}	10.3
Mode 9	2.8142×10^{-12}	2.7736×10^{-12}	−1.5
Mode 13	4.0043×10^{-12}	4.5064×10^{-12}	11.1
Mode 14	6.1628×10^{-12}	5.6929×10^{-12}	−8.3
Mode 19	3.5823×10^{-12}	4.1174×10^{-12}	13

stream line of the gas flows lead to a compact layer profile by closely packed particles. Measuring soot cake porosity using ex-situ instrumentation is troublesome and circumspect care should be given for sample preparation. Consequently, a model-based approach with a validated framework becomes a convenient method for the analysis of particle loading phenomena. In the present study, model formulation repeats the general frame developed in previous comprehensive modeling of DPF filtration by Konstandopoulos *et al.* (2002) with appropriate tailoring when needed.

A Brownian diffusion coefficient of an aerosol particle is expressed in terms of the properties of the particle and sustaining fluid by the Stokes-Einstein equation.

$$D=\frac{k_B\cdot T}{3\pi\cdot\mu\cdot d_{aggregate}}\cdot SCF_{aggreagate} \tag{8}$$

In Equation (8), k_B, μ, $d_{aggregate}$, and $SCF_{aggregate}$ are Boltzman's constant, gas viscosity, aggregate particle diameter and Stokes-Cunningham slip correction factor for aggregate particle, respectively. Deterministic modeling secures its uniqueness only when the participating physical parameters can be given in a deterministic manner again. The size of the particles contaminating the carrier gas stream may be defined by a single particle diameter. However, dealing with aggregate particle diameter correctly is not an easy task because the particles in the carrier gas stream behave in a stochastic fashion and thus may be highly uneven in their distribution with possibly a diverse composition; therefore, using a representative aggregate particle diameter based on the experimental observation rather than statistical means is judicious. As a fruit of much labor by many authors, a general profile of PM size distribution in diesel emissions are manifested in a number of reports. A general conclusion is particle distribution is narrowly banded and fractionates particles into two or more size categories of nuclei and accumulation modes (0.08 μm-0.2 μm). Mayer *et al.* (1996) reported that PM concentration consistently reaches its maximum at 0.08 μm~0.09 μm of PM size while showing little dependence on engine speed and mean pressure. This general profile has been solidly confirmed by many authors such as Shende *et al.* (2005) who reported that maximum diesel PM concentration appears in the vicinity of 0.15 μm of particle size with no significant deviation due to changes in engine loads. The results are elsewhere. Research recently conducted also show maximum concentration in the size range of 0.15 μm~0.2 μm, at a variety of operating modes (Liu *et al.*, 2002, 2003). Specifically, Harvey *et al.* (1994) investigated how the metallic additive in diesel fuel alters the profiles of PM concentrations in the carrier gas stream. Interestingly, with a different fraction of copper addition in the concentration range of 0 to 100 ppm, PM concentration due to heavy-duty diesel engines commonly show a peak at 0.15 μm of PM size. With such solid evidence, the present study uses the mean aggregate particle size ($d_{aggregate}$) of 0.1 μm, and also the primary particle size to compute soot cake porosity assumed to be 32.5 nm in diameter ($d_{primary}$). The present study assumes this geometry of particle size for the general framework of previous model studies (Konstandopoulos *et al.*, 2002;

Kladopoulou *et al.*, 2003) as a prerequisite for correct validation of the method in a quantitative manner. The other is that particles at accumulation mode take possession of a dominantly large fraction of particles in diesel exhaust gas; hence, the model may substitute aggregate particle size for an average. Regarding the number density, the distribution is overwhelmed by particles whose size is within the limits of nuclei mode. However, such superiority is heavily indebted to vast amounts of sulfate and hydrocarbon particles generated at the sampling stage of the dilution process for particle measurement. These illusive ingredients are carried in DPF flows during the gaseous state are forced into be condensed and very small particles in a sampled gas. This after-treatment effect may mislead understanding of phenomena and care should be given in order not to falsely count these sulfate and hydrocarbon particles.

As was aforementioned, the porosity and permeability, which is a target to expose the micro-structure of soot cake, depends on the Brownian diffusion coefficient of aggregate particles, convective velocity (filtration velocity), and primary particle size. Since the hydraulic resistance factor ($k_{soot}\rho_{soot,c}$) in Equation (6) is a unique parameter controlling the pressure drop in the soot cake mode, a strong correlation between the hydraulic resistance factor and soot cake Peclet number, defined as the ratio of convective to diffusive mass transport is expected.

$$Pe_{soot\ cake}=\frac{u_w \cdot d_{primary}}{D} \tag{9}$$

In Equation (9), convective transport characterized by soot cake porosity (primary particle diameter) is appropriate for low Reynolds number flows which are typical in filtration. It is noted that the aggregate particles command the diffusing process during the deep-bed period prior to the soot cake mode in which the particles are piled on the layer of the filter surface. Where a deep bed regime ends and a piling of particles was initiated, particles are transported into a particle latyer. Duering this soot cake regine, the filteration depends on the extent of gaseous convection and the quality of soot cake porosity.

Plots of the hydrodynamic resistance factor ($k_{soot}\rho_{soot,c}$) at different operation modes are shown in Figure 10. At all operation modes, the hydraulic resistance factors monotonically decrease with increase in the soot cake Peclet number and converge to the limiting value while reducing the degree of dispersion at high Pe numbers. Paralleled with an increase in Brownian diffusion (or decrease in Pe number), activation of irregular (wiggling) particle motion causes augmentation of soot cake porosity while lowering soot density. On the contrary, the hydrodynamic resistance factor soars higher at lower soot cake Peclet numbers due to an increase in permeability

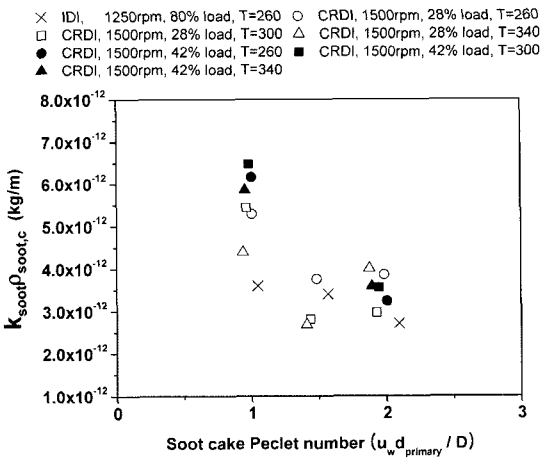

Figure 10. Experimental hydrodynamic resistance factors as a function of soot cake Peclet number.

superior to that of soot density. This Peclet number dependency has already been reported in the previous study (Konstandopoulos *et al.*, 2005). Authors believe however, that this strong correlation of hydrodynamic resistance factor to soot cake Peclet number should be firmly confirmed by more elaborate and refined experiments under a variety of cpnditions.

Nonetheless, the evaluation of soot cake porosity by mathematical descriptors of porous media is realized by inverse-analysis of measurements; uncertainties due to lack of explicit routes are left unclarified and to be tested. No evidence of repeatability and accuracy of the solutions are firmly presented yet, and quantitative validation is still required. However, it is generally accepted that the inverse-analysis yields qualitatively correct solutions with a physically consistent tendency, and thus it is expected that estimated soot cake porosity and its changes can be correctly projected on the resultant filtration performance. Permeability of porous media can be written as a function of a characteristic diameter of the collector element, a major structural component of porous media, and porosity function. Equation (10) provides a typical form of permeability equation for filtration by granular-type of collectors.

$$k_{soot}=C_{porous} \cdot f(\varepsilon) \cdot d_{primary}^2 \cdot SCF_{primary} \tag{10}$$

Here, C_{porous}, $f(\varepsilon)$ and $SCF_{primary}$ are a correction factor, Kuwabara porosity function, and Stokes-Cunningham slip correction factor for Stoke's law which accounts for the slip effect of a particle, respectively. Here, the correction factor and Kuwabara porosity function differ in their magnitude according to the composing substance of particles, thus are material-dependent functions. Evaluation of the slip correction factor is same as that for typical aerosol and calculated by an equation, $SCF = 1+Kn$

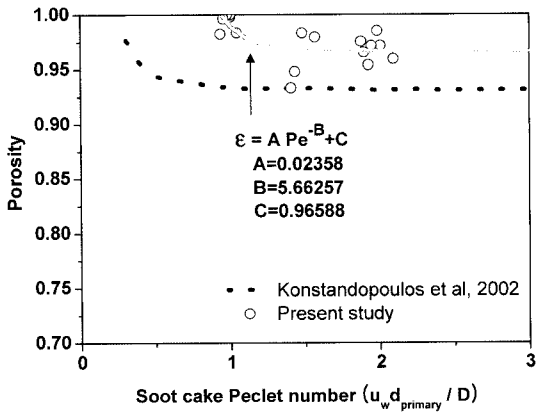

Figure 11. Soot cake porosity as a function of soot cake Peclet number. Solid line which fits the measured data and corresponds to porosity-Peclet number relation (Equation 12), is compared with the reference (Konstandopoulos *et al.*, 2002).

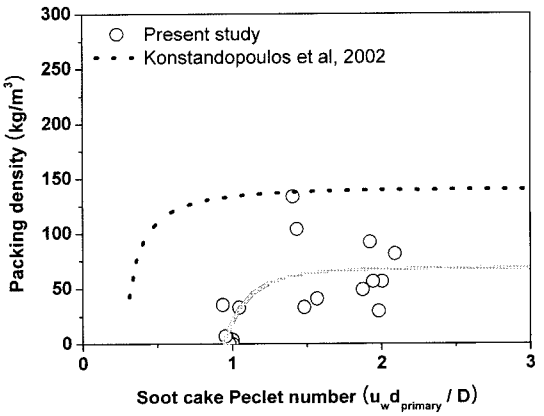

Figure 12. Soot packing density as a function of soot cake Peclet number. Solid line which fits the measured data and is inversely proportional to the soot cake porosity (Figure 11), is compared with the reference (Konstandopoulos *et al.*, 2002).

$(1.257+0.4\exp(-1.1/Kn))$ with $Kn = 2\lambda/d_{primary}$. Previous studies assumes C_{porous} being unity but with lack of reliable evidence, and the present study repeats this value for simplicity. Soot packing density is defined as a non-porous fraction of the volume.

$$\rho_{soot,c}=\tilde{\rho}\cdot(1-\varepsilon) \tag{11}$$

Here, $\tilde{\rho}$ is density of a solid carbon and approximately 2000 kg/m^3. With a set of experimentally determined hydrodynamic resistance factors (Table 2), soot cake porosity, packing density and permeability were inversely analyzed until the relations in Equations (10), (11) were fulfilled within limits. Figure 11 depicts the dependence of soot cake porosity on the soot cake Peclet number. At all test modes, degrees of dispersion are low and porosities are of values higher than 0.93. Soot cake porosity reaches its maximum in the vicinity of $Pe \approx 1$ where, paralleled with convective deposition, contribution of Brownian diffusion to particle deposition becomes equally important. In Figure 11, a porosity curve drawn with solid line which fits the analysis data, provides an approximate functional expression of the soot cake porosity in relation to the Peclet number.

$$\varepsilon=A\cdot Pe^{-B}+C \tag{12}$$

Functional representation which is amenable to mathematical interpretation like Equation (12), has been originally introduced by stochastic particle simulation (Tassopoulos, 1991) in order to estimate particle deposition and layer porosity due to convective-diffusive transportation of particles. It is expected that porosity attains an asymptote around 0.97, which is somewhat different from the experimentally obtained value of 0.93 in a previous study (Konstandopoulos *et al.*, 2002).

Dependence of soot packing density on soot cake Peclet number is also investigated. As shown in Figure 12, the fitted curve mimics the capsized shape of that of Figure 11, and the ordinate is now the soot packing density. The soot packing density monotonically increases with increasing soot cake Peclet number and converges to a limiting value of around 70 kg/m^3, while reducing the degree of dispersion moderately at high Peclet numbers. Previous reports mentioned that in addition to Peclet number dependency, augmentation of packing level due to compression effects becomes substantial at soot cake mode with pressure drop over 20 kPa (Sorenson *et al.*, 1994; Konstandopoulos *et al.*, 2005). However, compaction of soot cake is not intended in the present study because, PM loading is conducted with pressure drops less than 20kPa and thus compression effects are not distinct in the present single channel DPF experiments.

Figure 13 compares measured soot cake permeability with analytical results (solid lines) evaluated by a porosity-Peclet number correlation (Equation 12) at three different temperatures. The degree of data dispersion is very high in the vicinity of Pe1 and the variation at soot cake Peclet numbers higher than unity is within fractional limit. Higher gas temperature is equivalent to an increment of a gas molecule's mean free path and is thus, the Knudsen number. Flow field around packed beds evaluated theoretically with gas slippage effects, revealed that the pressure loss is alleviated at higher Knudsen number, and thus augmentation of permeability is expected (Lee *et al.*, 1978). This temperature effect is not noticeable in measured data whereas a slight increase in permeability due to a temperature rise is observed in Figure 13.

Dependence of soot density in the filter wall on the filter wall Peclet number is shown in Figure 14. Much the

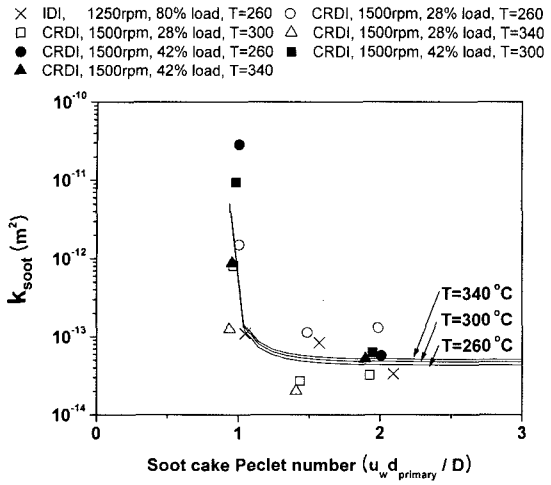

Figure 13. Soot cake permeability as a function of soot cake Peclet number. Model permeability (solid lines) with due premises of porosity-Peclet number relation in Figure 11 combined with Equation 10 at three temperatures of 260°C, 300°C, and 340°C shows weak temperature-dependence.

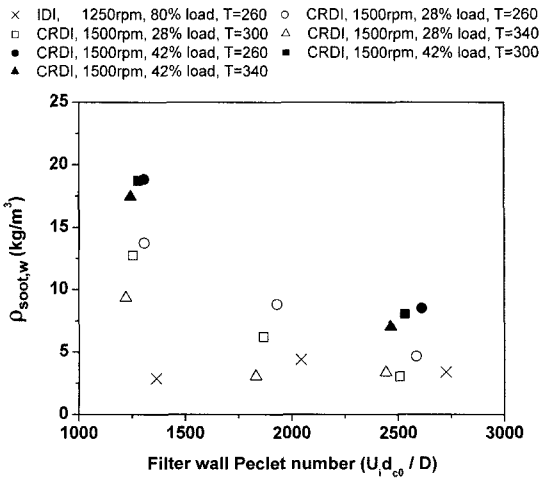

Figure 14. Soot density in the filter wall as a function of filter wall Peclet number at different engine operation modes.

same as previous selection of parameters for defining the soot cake Peclet number (Equation 9), Brownian motion of particles is assumed to be controlling the diffusive transport. However, characteristic length and velocity for convective transport are replaced by a collector diameter and interstitial velocity, respectively.

$$Pe_{filter\ wall}=\frac{U_i \cdot d_{c0}}{D} \tag{13}$$

In Equation (13), U_i and d_{c0} are interstitial (or pore) velocity (u_w/ε) and clean filter collector diameter, respectively. A profile of soot density in the filter wall with respect to filter wall Peclet number is similar to that of the hydrodynamic resistance factor to soot cake Peclet number. Contrary to augmentation of soot packing density for strengthening the convection, soot density in the filter wall decreases as the filter wall Peclet number increases. This is not physically acceptable, since, as was previously outlined, soot density in the filter wall is not physically defined. Therefore, speculating the filtration mechanism on the basis of soot density in the filter wall leads to a non-physical situation. Though soot density in the filter wall is bounded between 3 and 10 kg/m^3 at high filter wall Peclet numbers, this high Peclet number asymptote must be firmly ascertained by more elaborate and refined experiments.

6. SENSITIVITIES OF FILTRATION PARAMETERS TO MODE TRANSITION

Targeting the sensitivity analysis of model parameters relevant to a transition regime from deep-bed to soot cake filtration modes, parametric studies on the effects of soot density in the filter wall ($\rho_{soot,w}$) and percolation constant (ψ) were performed. In Figure 15, evolving pressure drops due to different soot densities in the filter wall ($\rho_{soot,w}$) are compared by predicted (solid lines) and measured (solid square) data plots. In this parametric diagnosis, the soot density in the filter wall can vary in the range of ±20% from a reference quantity of mode 14. Obviously, the quality of soot density in the wall significantly alters the temporal grade of transition, i.e. the rate of change in pressure drop rises in proportion to a rise in the specific volume of the soot inside the filter wall so

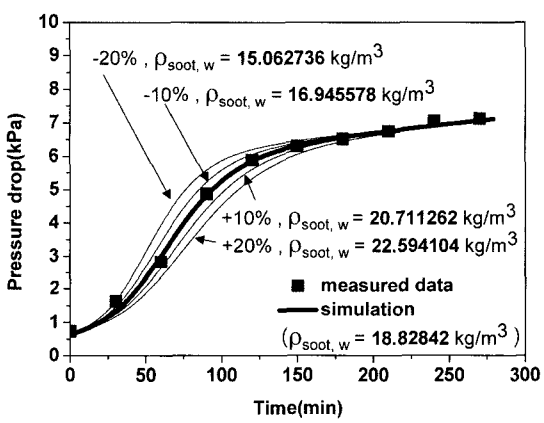

Figure 15. Sensitivity of pressure drop to soot density in the filter wall for mode 14. Thick solid line is model prediction with base values of filtration parameters. For the sake of probing sensitivity, soot density in the filter wall is forced to be deviated in the range of (thin solid line) from reference quantity (thick line).

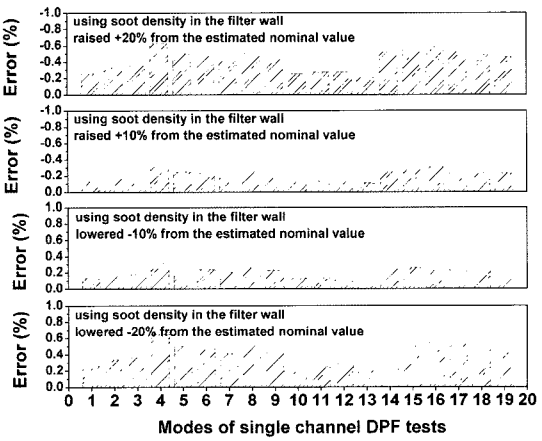

Figure 16. Error percentages to estimate the relative importance of soot density in the filter wall in terms of engine operation mode.

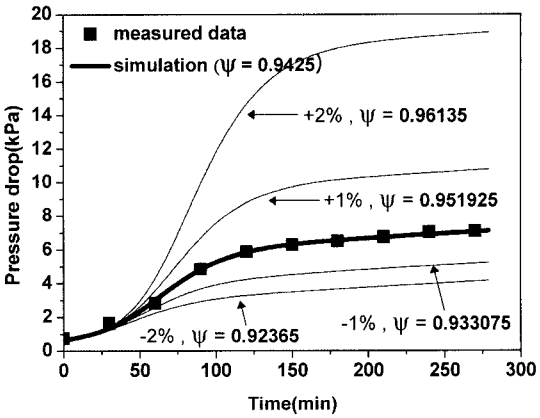

Figure 17. Sensitivity of pressure drop to percolation constant for mode 14. Thick solid line is model prediction with base values of filtration parameters. For the sake of probing sensitivity, soot density in the filter wall is forced to be deviated in the range of (thin solid line) from the reference quantity (thick line).

that the mode of transition to soot cake mode is expedited. However, regardless of fairly different transition histories, the loading quality for the soot cake mode is unaffected by the extent of soot density in the filter wall and thus the pressure drops at the terminating stage of PM loading (soot cake mode) commonly tend to be straitened. Loading characteristic by DPF seems insensitive to changes in $\rho_{soot,w}$. This is repeatedly shown in Figure 16, which puts the error percentage of predicted loading pressure drop, deviated from a measured reference into a histogram of different test modes and soot density in the filter wall; deviations caused by changes in soot density in the filter wall are confined within 1% and their profiles are all alike irrespective of the operation modes. Conclusively, the soot density in the filter wall is essential to rate-controlling of the mode transition but has less influence on the pressure drop.

Another sensitivity analysis is given by the percolation constant while employing a general framework used in the case of soot density in the filter wall. In Figure 17, evolutions of pressure drop due to changes in the magnitude of the percolation constant (ψ) are compared in a similar manner. For a percolation constant, deviations are narrowly limited within ±2% of reference quantity by mode 14. Figure 18 repeats Figure 16 but the ordinate is replaced with the percolation constant as a dependent variable. Contrary to the inertness of the pressure drop to the soot density in the filter wall, pressure drops are greatly altered by small changes in the percolation constant. Only 1% increase from the reference causes a 25% increase in the resultant pressure drop, and its extent of contribution is vastly augmented to 150% by a 2% increase. Evidently, the model is very sensitive to the input value of a percolation constant and great care must be exercised in its evaluation.

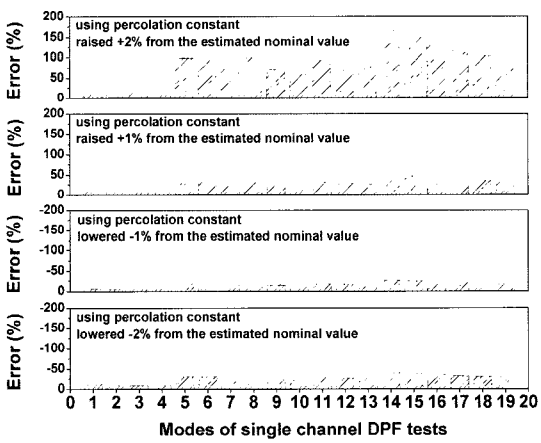

Figure 18. Error percentages to estimate the relative importance of percolation constant in terms of engine operation mode.

Interestingly, the percolation constant is not a strong function of the filter wall Peclet number, which commands a diffusion pattern and thus, is not significantly altered during a fixed test mode. Figure 19 plots the percolation constants under three groups of operation conditions: 1250 rpm-80% load, 1500 rpm-28% load, and 1500 rpm-42% load. Clearly, the percolation constant is inert to changes in the volumetric flow rate or temperature of exhaust gas, while maintaining its changes less than 1%. Figure 20 illustrates the error percentage of a termination pressure drop by the histogram for different test modes. For all test modes, the model initialized with averaged percolation constants shown in Figure 19, causes a prediction error of less than 15%.

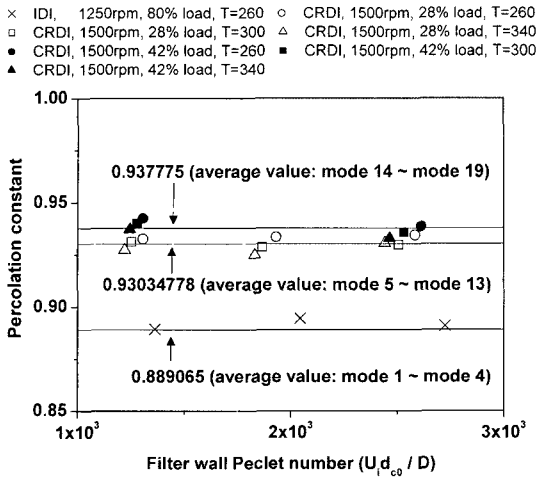

Figure 19. Percolation constant and its average for three engine operating modes as a function of filter wall Peclet number (mode 1~4: 1250 rpm-80% load, mode 5~13: 1500 rpm-28% load, and mode 14~19: 1500 rpm-42%). One data point of mode 1 is beyond the limit of ordinate but considered in average value accounts.

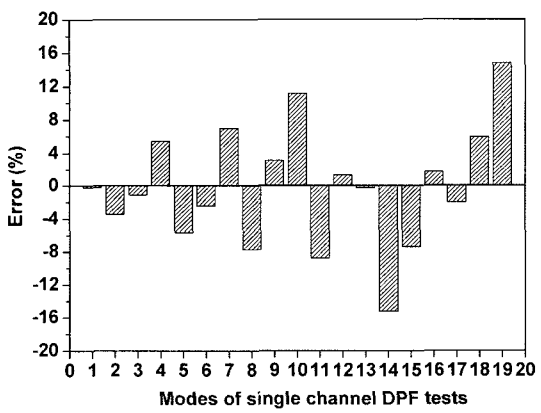

Figure 20. Error percentages of the predicted pressure drop at the end of loading in terms of engine operation mode. (Calculation was made with averaged percolation constants shown in Figure 19).

7. CONCLUSIONS

The aim of this study is to estimate important filtration parameters, essential to a mathematical interpretation of evolving pressure drops. DPF filtration modeling with a non-linear regression scheme was attempted. The data obtained from a series of single channel DPF tests were inversely analyzed in order for computationally deducting filtration parameters. Dependence of soot cake porosity, packing density, permeability, and soot density in filter wall on convective-diffusive particle transportation was examined. In addition, sensitivity analysis of soot cake density in the filter wall and of a percolation constant was conducted.

(1) The degree of dispersion of soot cake porosity with respect to the Peclet number is low and the porosity has its asymptote of 0.97, at high Peclet numbers. Soot packing density increases monotonically with soot cake Peclet number and attains a limit at 70 kg/m^3. The degree of data dispersion is very high in the vicinity of $Pe \approx 1$ and the variation at soot cake Peclet numbers higher than unity is gradual and within a fractional limit.

(2) Soot density in the filter wall decreases as the filter wall Peclet number increases and is bounded between 3 and 10 kg/m^3 at high filter wall Peclet numbers.

(3) Soot density in the filter wall is essential to the rate-controlling of the filtration mode transition; however, the loading quality at the soot cake mode is practically unaffected. Profiles of pressure drops are significantly altered by small changes to the percolation constant and great care should be devoted to the filtration model, requiring assistance with its correct and accurate estimation. The percolation constant is inert to changes in the volumetric flow rate or the temperature of exhaust gas at fixed operation mode.

ACKNOWLEDGEMENT–This work has been done in part of the research project 'Development of Partial Zero Emission Technology for Future Vehicle'. We are grateful of its supports.

REFERENCES

Bissett, E. J. (1984). Mathematical model of the thermal regeneration of a wall-flow monolith diesel particulate filter. *Chemical Engineering Science*, **39**, 1233–1244.

Harvey, G. D., Baumgard, K. J., Johnson, J. H., Gratz, L. D., Bagley, S. T. and Leddy, D. G. (1994). Effects of a ceramic particle trap and copper fuel additive on heavy-duty diesel emissions. *SAE Paper No.* 942068.

Hinds, W. C. (1999). *Aerosol Technology: Properties, Behavior and Measurement of Airborne Particles.* 2nd edn. John Wiley & Sons. New York.

Huynh, C. T., Johnson, J. H., Yang, S. L., Bagley, S. T., and Warner, J. R. (2003). A one-dimensional computational model for studying the filtration and regeneration characteristics of a catalyzed wall-flow diesel particulate filter. *SAE Paper No.* 2003-01-0841.

Kladopoulou, E. A., Yang, S. L., Johnson, J. H., Parker, G. G., and Konstandopoulos, A. G. (2003). A study describing the performance of diesel particulate filters during loading and regeneration-A lumped parameter model for control application. *SAE Paper No.* 2003-01-0842.

Konstandopoulos, A. G. and Johnson, J. H. (1989). Wall-flow diesel particulate filters-Their pressure drop and

collection efficiency. *SAE Paper No.* 890405.

Konstandopoulos, A. G., Kostoglou, M., Skaperdas, E., Papaioannou, E., Zarvalis, D. and Kladopoulou, E. A., (2000). Fundamental studies of diesel particulate filter: Transient loading, regeneration and aging. *SAE Paper No.* 2000-01-1016.

Konstandopoulos, A. G., Skaperdas, E. and Masoudi, M. (2001). Inertial contributions to the pressure drop of diesel particulate filters. *SAE Paper No.* 2001-01-0909.

Konstandopoulos, A. G., Skaperdas, E. and Masoudi, M. (2002). Microstructural properties of soot deposits in diesel particulate traps. *SAE Paper No.* 2002-01-1015.

Konstandopoulos, A. G. (2003). Flow resistance descriptors for diesel particulate filters: Definitions, measurements and testing. *SAE Paper No.* 2003-01-0846.

Konstandopoulos, A. G., Kostoglou, M., Vlachos, N. and Kladopoulos, E., (2005). Progress in diesel particulate filter simulation. *SAE Paper* No. 2005-01-0946.

Lee, K. W., Reed, L. D. and Gieseke, J. A. (1978). Pressure drop across packed beds in the low Knudsen number regime. *J. Aerosol Sci.*, **9**, 557–565.

Liu, Z. G., Verdegan, B. M., Badeau, K. M. A. and Sonsalla, T. P. (2002). Measuring the fractional efficiency of diesel particulate filters. *SAE Paper No.* 2002-01-1007.

Liu, Z. G., Skemp, M. D. and Lincoln, J. C. (2003). Diesel particulate filters: Trends and implications of particle size distribution measurement. *SAE Paper No.* 2003-01-0046.

Mayer, A., Czerwinski, J. and Scheidegger, P. (1996). Trapping efficiency depending on particulate size. *SAE Paper No.* 960472.

Opris, C. N. and Johnson, J. H. (1998). A 2-D computational model describing the flow and filtration characteristics of a ceramic diesel particulate trap. *SAE Paper No.* 980545.

Opris, C. N. and Johnson, J. H. (1998). A 2-D computational model describing the heat transfer, reaction kinetics and regeneration characteristics of a ceramic diesel particulate trap. *SAE Paper No.* 980546.

Park, J. S. (2005). *A Study on the Relation between PM Loading and Pressure Drop Using Single Channel DPF.* M. S. Thesis. Yonsei University. Seoul. Korea.

Park, J. S., Yoon, C. S, Lee, H. S. and Chun, K. M. (2005). A study on the relation between PM loading and pressure drop using single channel DPF. *Spring Conf. Proc., The Korean Society of Automotive Engineers*, 247–252.

Press, W. H., Teukolsky, S. A., Vetterling, W. T. and Flannery, B. P. (1992). *Numerical Recipes.* The Art of Scientific Computing. 2nd edn. Cambridge University Press. Cambridge.

Shende, A. S., Johnson, J. H., Yang, S. L., Bagley, S. T., and Thalagavara, A. M. (2005). The filtration and particulate matter oxidation characteristics of a catalyzed wall-flow diesel particulate filter: Experimental and 1-D 2-layer model results. *SAE Paper No.* 2005-01-0949.

Sorenson, S. C., Hoj, J. W. and Stobbe, P. (1994). Flow characteristics of SiC diesel particulate filter materials. *SAE Paper No.* 940236.

Tassopoulos, M. (1991). *Relationships between Particle Deposition Mechanism, Deposition Microstructure and Effective Transport Properties.* Ph.D. Dissertation. Yale University. USA.